

Pressure compensated fiber laser hydrophone: Modeling and experimentation

Unnikrishnan Kuttan Chandrika^{a)} and Venugopalan Pallayil
Acoustic Research Laboratory, National University of Singapore, Singapore 119227

Kian Meng Lim and Chye Heng Chew
Department of Mechanical Engineering, National University of Singapore, Singapore 117576

(Received 26 February 2013; revised 2 July 2013; accepted 9 August 2013)

A pressure compensated metal diaphragm based fiber laser hydrophone configuration that can provide good sensitivity, large bandwidth, and sea state zero noise floor is proposed in this paper. A simplified theoretical model of the proposed sensor configuration is developed in which the acoustic elements of the sensor configuration are modeled using a four-pole acoustic transfer matrix and the structural elements are modeled as second order single degree of freedom elements. This model is then used to optimize the design parameters of the sensor system to achieve the performance objectives. An axisymmetric finite element analysis of the sensor configuration is also carried out to validate the results from the simplified theoretical model. Prototype sensors were fabricated and hydrostatic testing in a pressure vessel validated the static pressure compensation performance of the sensor. Frequency dependent sensitivity of the sensor system was measured through acoustic testing in a water tank. The prototype sensor gave a flat frequency response up to 5 kHz and experimental results compared well with theoretical predictions. The sensor has an acceleration rejection figure on the order of 0 dB ref 1 m/s² Pa and the pressure compensation approach worked reasonably well up to a hydrostatic pressures equivalent to a depth of 50 m.

© 2013 Acoustical Society of America. [<http://dx.doi.org/10.1121/1.4819120>]

PACS number(s): 43.30.Yj, 43.20.Ye, 43.40.At [DDE]

Pages: 2710–2718

I. INTRODUCTION

Fiber optic hydrophones using Bragg reflectors and fiber lasers have been explored as an alternatives to conventional ceramic based hydrophones due to its many advantages such as high sensitivity to strain, immunity to electromagnetic interference, intrinsic safety to water leakage, ease of multiplexing and remote measurement capability.^{1–3} The fiber laser based hydrophone (FLH) technology has been fast developing and it may soon replace the existing mandrel wound fiber optic hydrophones due to their high sensitivity and compact size. Though not widely addressed in open literature, an important area that requires special attention is in the design of a suitable encapsulation for these hydrophones so that they can be safely deployed in seawater. A well designed encapsulation is also important to enhance the sensitivity and frequency response characteristics of fiber laser hydrophones.

Even though the wavelength of fiber laser output is highly sensitive to strains, high elastic modulus of the glass fiber necessitates methods to enhance the pressure sensitivity of the fiber laser. Most of the initial works toward the sensitivity improvements focused on the application of compliant coatings^{4–6} and rubber diaphragms.⁷ Significant sensitivity improvements could be achieved through these methods, yet the operational bandwidth of these sensors were limited by the low natural frequency of the active sensing region. Polymer based compliant coatings also has to go through a

curing process before it settles and this often resulted in uneven strains to be applied on the sensor grating structure. Hence as the curing process progresses the wavelength tends to shift from its designed value before settling into a new final value at the completion of the curing process.⁸ It has also been observed that the strains developed during curing process sometimes results in the damage of the grating structure and thereby destroying the sensor itself.⁴ The third aspect to be considered when designing the encapsulation is the safe operating depth of the sensor system which often calls for the use of a pressure compensation system that would null the effect of static pressure on the sensor. In the absence of a pressure compensation system, the strain due to static pressure could shift the laser wavelength to one end and thus reducing the effective dynamic range or even push the laser wavelength out of the detection band. Foster *et al.*⁹ presented a fiber laser hydrophone configuration, which works in bending mode and has an operational bandwidth of 0–2.5 kHz. Later on Goodman *et al.*¹⁰ incorporated an external air bladder for pressure compensation of the bending mode DFB fiber laser hydrophone to achieve safe operating depths on the order of 50 m. Another fiber laser hydrophone with good acceleration rejection characteristics and improved frequency range of operation, though not pressure compensated, was reported by Foster *et al.*¹¹ An integrated approach to the design of encapsulation that addresses the sensitivity, pressure compensation, and wide bandwidth of operation and related theoretical framework is not available in open literature to the best of our knowledge. This work presents a miniature pressure compensated metal diaphragm based fiber laser hydrophone capable of measuring acoustic

^{a)}Author to whom correspondence should be addressed. Electronic mail: unni@arl.nus.edu.sg

signals as small as sea state zero noise levels and a flat frequency response in frequency range 10 Hz to 5 kHz. The pressure compensation technique implemented has been found to work reasonably well for up to a depth of 50 m. This paper has been organized into three main sections. In Sec. II, an overview of the design considerations of a fiber laser hydrophone in conjunction with the most widely used detection methodology is presented. The proposed design approach for the new FLH is described in Sec. III. A theoretical framework developed for the FLH encapsulation and its validation through finite element analysis (FEA) is described in Sec. IV. Finally, the test results on acceleration sensitivity, pressure compensation, frequency response and its comparison with those predicted by the models are presented in Sec. V. The paper concludes with a summary of our findings.

II. DESIGN CONSIDERATIONS OF FIBER LASER HYDROPHONE

Fiber laser hydrophones work based on the principle that the pressure changes due to an acoustic wave will introduce corresponding changes in the wavelength of the laser generated by the fiber laser. Interferometric systems are usually employed to convert the wavelength shifts in the fiber laser output into light intensity variations, which can then be converted to electrical signals using photo receivers.⁴ The design parameters of FLH system considered in the current study are its sensitivity, frequency response, measurement resolution, dynamic range, and harmonic distortion.

The phase resolution and noise floor characteristics of the fiber laser hydrophone system depend directly on three major parameters: The measurement resolution of the opto-electronic instrumentation, the inherent frequency noise of the fiber laser and the optical path imbalance used in the interferometer. Commercial phase demodulation systems that can achieve measurement resolutions on the order of a few micro radians are available off the shelf. Thus for a fiber laser sensor with sufficient phase sensitivity to generate phase changes greater than the measurement resolution of the opto-electronic instrumentation, the noise floor is primarily dictated by the inherent noise from the fiber laser.¹² The phase sensitivity of fiber laser hydrophone can be defined as the phase change produced per unit pressure and can be expressed as¹²

$$\frac{\partial \phi}{\partial P} = \frac{nkD}{\lambda} \eta \quad (1a)$$

where

$$\eta = -\frac{1}{P} \frac{d\lambda}{\lambda} = \frac{1}{P} \frac{dF_L}{F_L} \quad (1b)$$

In Eq. (1), n is the refractive index, k is the wave number, and η is the pressure sensitivity of the active sensing region, D is the optical path imbalance in the interferometer, and P is the pressure that produces a corresponding wavelength change of $d\lambda$ in the fiber laser wavelength λ (or frequency change dF_L in the fiber laser frequency F_L). The DFB fiber laser used in the study consists of a 35 mm

long π -phase-shifted grating written on an Erbium–Ytterbium doped fiber. Application of this sensor in a quiet environment demands the sensor to have sufficient mechanical sensitivity such that the frequency changes due to ambient acoustic noise is greater than the frequency noise floor of the fiber laser. Thus, for a phase noise value of $62 \text{ Hz}/\sqrt{\text{Hz}}$ at 1 kHz estimated from measurements, the pressure sensitivity (η) should be greater than $2 \times 10^{-9} \text{ Pa}^{-1}$ to produce measurable phase changes in sea state 0 noise environments where the ambient noise levels are as low as $160 \mu\text{Pa}/\sqrt{\text{Hz}}$ at 1 kHz.¹³ As optical fibers have a very large elastic modulus, the resultant pressure sensitivity is only $2.5 \times 10^{-12} \text{ Pa}^{-1}$. Compliant mechanical packaging, which leads to a reduction in the stiffness of the active sensing region, is often employed to improve the sensitivity. However, reducing the stiffness also lowers the fundamental natural frequency of the active sensing region thus lowering the fundamental natural frequency of the active sensing region. It is desirable to have the resonances well away from the operating band to ensure a flat frequency response. Hence to achieve the performance objective of high and flat sensitivity over a large frequency range, the stiffness of the active sensing region need to be optimized while minimizing the mass associated with the fundamental mode of vibration.

The distortion free dynamic range of the fiber optic hydrophones directly depends on the phase sensitivity of the hydrophone system [Eq. (1a)] and phase modulation schemes employed. Phase generated carrier (PGC) schemes are often used in opto-electronic instrumentations for underwater acoustic sensing applications, as it is capable of achieving high dynamic range and fine phase resolutions. Phase generated carrier—differentiation and cross multiplication (PGC-DCM) and PGC-Arctangent schemes are the most widely used among them. Many variants of these techniques have also been developed in the past to address the harmonics and signal distortions associated with the fiber laser light intensity noise and errors associated with the modulation depth.^{14–16} These schemes enable us to achieve total harmonic distortion (THD) factors smaller than 0.1% (harmonic suppression >60 dB), provided sufficiently high enough carrier frequency is employed. As a general rule it could be stated that, for a given carrier frequency, THD values can be minimized by using lowest possible phase sensitivity value that meets the phase resolution requirements of the sensor. As the pressure sensitivity of the active sensing region directly depends on the frequency noise of the fiber laser output, the optical path difference in the interferometer is the only major independent parameter [in Eq. (1a)] that determines the distortion free dynamic range and sensitivity of the sensor. The sensor system should also need to be made insensitive to hydrostatic pressure. At a typical operational depth the hydrostatic pressure could be many orders greater than the acoustic pressure and a high mechanical sensitivity could lead to large shifts in the wavelength. This is a problem in multi-channel sensor array as it could result in the overlapping of channels. In some cases lack of pressure compensation may lead to structural failures under the action of hydrostatic pressures. Though external pressure compensation techniques could be applied, integrating the pressure

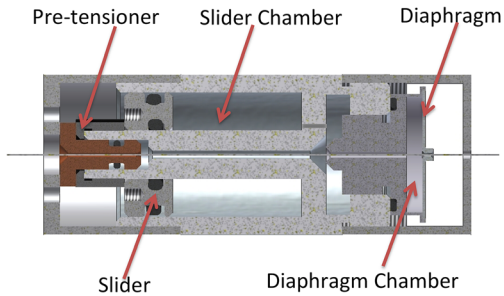


FIG. 1. (Color online) Design configuration of the FLH prototype.

compensation scheme into the encapsulation could lead to a more compact and less complex sensor configuration.

III. DESIGN CONFIGURATION OF THE PROPOSED HYDROPHONE

A design configuration where a thin metallic plate acts as a mechanical diaphragm as shown in Fig. 1 is proposed in this work to achieve the performance objectives specified in the previous section. A distributed feedback fiber laser (DFB-FL) is centrally placed inside the aluminum packaging with one end of the fiber attached to a thin mechanical plate and the other end to a pre-tensioning arrangement. The pre-tension arrangement, which consists of a sleeve mounted on threaded connection to the sensor shell, ensures the adjustment of the pre-tension on the fiber without introducing torsional strain. The application of pretension eliminates the string modes of the fiber laser in the frequency range of interest and reduces the vibration sensitivity of the sensor. The diaphragm-based design amplifies the strain introduced on the fiber by effectively increasing the active sensing area of the sensor. The deflection of the diaphragm due to the acoustic pressure variations will impart corresponding strain on the fiber, which is measured as a shift in the frequency or wavelength of fiber laser output. The slider arrangement ensures the static pressure compensation by altering the slider chamber volume proportionately with the operating depth. It is also necessary to ensure that the acoustic sensitivity of the fiber laser hydrophone is not affected by the pressure compensation scheme. Hence the air chamber behind the diaphragm is connected to the slider chamber through an acoustic low pass filter which ensures that only very low frequency pressure changes are allowed to pass into the diaphragm chamber.

IV. THEORETICAL MODEL AND PERFORMANCE PREDICTION

The sensitivity and frequency response characteristics of the proposed design configuration are decided by the following parameters: Stiffness of the diaphragm, stiffness of the fiber, stiffness of the molding used to attach the DFB-FL to packaging, frequency response characteristics of the pressure compensation systems and effective mass of the fundamental mode of vibration of the active sensing region. As there are multiple design parameters that need to be optimized to achieve the design objectives, it would be ideal to have a theoretical model of the fiber laser hydrophone system. As the acoustic wavelengths of interest are much larger than dimensions of the sensor under considerations, it allows the modeling of the

acoustic components of the sensor system using one dimensional wave equation. A theoretical model of the fiber laser hydrophone as represented in Fig. 2 and consisting of mainly three components, namely, acoustic filter, slider, diaphragm is discussed in the following sections. This model will be used to study the effect of design parameters on sensor performance and selection of optimum values for those parameters.

A. Acoustic filter

Acoustic filter of the sensor consists of five acoustic elements as marked in Fig. 2. Acoustic element 1 represents the slider chamber and its volume decides the operational depths up to which effective pressure compensation can be achieved. Elements 3 and 5 represent the expansion chamber and the diaphragm chamber, respectively. The sections 2 and 4 represents the links that connect the expansion chamber to the slider chamber and diaphragm chamber, respectively. An acoustic four-pole method offers a suitable tool for modeling of the sensor system as it consists of acoustic elements that could be accurately modeled using 1-D wave equations and structural elements that can be approximated using single degree of freedom second order systems. In acoustic four-pole method, the characteristics of individual sections or elements of sensor system are formulated in the form of transfer matrix, which relates the pressure and volume velocity at the input to pressure and volume velocity at the output. Thus, four-pole method allows the individual sections of the sensor to be independently modeled and then multiplied together to get the combined transfer matrix of the sensor. Figure 3 shows a schematic of a linear acoustic duct system of length L and cross section area S . The four-pole equation for this system can be expressed as¹⁷

$$\begin{bmatrix} P(0) \\ Q(0) \end{bmatrix} = [T] \begin{bmatrix} P(L) \\ Q(L) \end{bmatrix} \quad (2a)$$

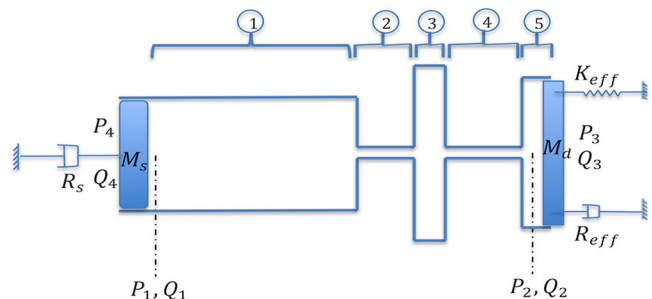


FIG. 2. (Color online) Schematic of the simplified sensor model.



FIG. 3. Linear acoustic 1-D element.

where

$$[T] = \begin{bmatrix} \cos(kL) & j\left(\frac{\rho c}{S}\right) \sin(kL) \\ j\left(\frac{S}{\rho c}\right) \sin(kL) & \cos kL \end{bmatrix}. \quad (2b)$$

In Eq. (2) P is the pressure and Q is the volume velocity, ρ is the density, c is the velocity of sound and k is the complex wave number as expressed in Eq. (3).¹⁸

$$k = \frac{\omega}{c} - j\frac{\sigma}{2\rho c} \quad (3)$$

In Eq. (3), flow resistivity σ accounts for the viscous losses in the duct. For circular ducts of radius a containing a fluid with dynamic viscosity μ , value of flow resistance can be expressed as in Eq. (4).¹⁸

$$\sigma = \frac{8\mu}{a^2}. \quad (4)$$

Thus using Eqs. (3) and (4), the effective transfer characteristic of the acoustic filter section can be written as in Eq. (5) where $[T_1]$ to $[T_5]$ are the transfer functions corresponding to acoustic elements marked 1–5 in Fig. 2.

$$\begin{bmatrix} P_1 \\ Q_1 \end{bmatrix} = [T_1][T_2][T_3][T_4][T_5] \begin{bmatrix} P_2 \\ Q_2 \end{bmatrix}. \quad (5)$$

B. Slider

The two major sources of energy dissipation at the slider are frictional loss at the O-ring interface and acoustic radiation loss to surrounding water arising from the motion of the slider. Only dynamic friction effects of O-ring sealing at the slider–slider chamber interface is considered in the analysis, as the static friction at the interface will only introduce a fixed pressure imbalance between the outside environment and the slider chamber. The frictional loss happening at the O-rings were incorporated into the slider model using equivalent damping coefficient.¹⁹ The radiation loss at the slider can be written as in Eq. (6) (Ref. 20) where S_s is the area of slider, a_s is the radius of the slider, ρ_w is the density of water, and c_w is the velocity of sound in water. As the slider motion happens in water, the added mass effect also needs to be

considered. Hence total mass M_s associated with the slider motion can be written as in Eq. (7) where m_s is the mass of the slider.²⁰

$$R_s = \frac{1}{2}\rho_w c_w S_s (k_w a_s)^2 \quad (6)$$

$$M_s = m_s + \frac{8}{3}\rho_w a_s^3. \quad (7)$$

Assuming uniform pressure acts over the entire area of the slider, its transfer characteristics can be written as

$$\begin{bmatrix} P_4 \\ Q_4 \end{bmatrix} = [T_s] \begin{bmatrix} P_1 \\ Q_1 \end{bmatrix}, \quad (8a)$$

where

$$[T_s] = \begin{bmatrix} 1 & \left(\frac{j\omega M_s + R_s + C_{eq}}{S_s^2}\right) \\ 0 & 1 \end{bmatrix}. \quad (8b)$$

In Eq. (8), P_1 and P_4 represent the pressures acting on slider as shown in Fig. 2.

C. Diaphragm

The active sensing region of the sensor system consists of a fiber laser that is mounted centrally through a thin circular plate using a high modulus adhesive. The thin circular plate constrained at its outer diameter is exposed to water on one side and air on the other. The entire active sensing region can be represented by a single degree of freedom system as represented in Fig. 2. The effective stiffness K_{eff} of the model as expressed in Eq. (9) can be derived using the formulae for deflection of a circular plate under the action of uniform pressure and concentrated force.²¹ In Eq. (9), E_d and E_f are the Young's modulus of the diaphragm and fiber, respectively, h is the diaphragm thickness, a_d is the diaphragm radius, ν_d is the Poisson's ratio for the diaphragm material, S_f is the cross section area of the fiber, and L_f is the length of the fiber.

$$K_{eff} = \frac{64\pi E_d h^3}{3a_d^2(1-\nu_d^2)} + \frac{4E_f S_f}{L_f} \quad (9)$$

$$Q_3 = 0.309 S_d u_c \quad (10)$$

$$M_d = 0.309 \left(m_d + \frac{8}{3}\rho_w a_d^3 \right). \quad (11)$$

The major source of energy dissipation at the diaphragm is the radiation loss to surrounding water. The radiation loss at the diaphragm depends on the effective volume flow rate at the diaphragm, and it can be calculated using the average velocity of the diaphragm. For a vibrating circular plate of an area S_d and constrained at the boundary, the average volume flow rate can be written as in Eq. (10) where u_c is the velocity amplitude at the center. The factor 0.309 in Eq. (10) originated from the integration of the mode shape of the

fundamental mode of vibration, which is essentially a Bessel function of first kind.²² The total mass associated with motion of the diaphragm can then be expressed as in Eq. (11).

Thus the transfer characteristics of the active sensing region can be written as

$$\begin{bmatrix} P_2 \\ Q_2 \end{bmatrix} = [T_d] \begin{bmatrix} P_3 \\ Q_3 \end{bmatrix}, \quad (12a)$$

where

$$[T_d] = \begin{bmatrix} 1 & -\left(\frac{j\omega M_d + R_d - K_{eff}}{S_d^2}\right) \\ 0 & 1 \end{bmatrix}. \quad (12b)$$

In Eq. (12), R_d is the radiation loss at the diaphragm which can be calculated using an expression similar to Eq. (6).

D. Sensor model

The transfer characteristics of the sensor can be expressed as a combination of the transfer function for the filter, slider, and the diaphragm as given in Eq. (13). It can be assumed that $P_4 = P_3 e^{j\theta}$ and $\theta \approx 0$ as the dimensions of the sensor is much smaller in comparison to the acoustic wavelengths of interest. Thus, the effective strain, ε on the fiber can be derived as in Eq. (14) using Eqs. (13) and (10). For a fiber laser under the action of axial strain, the pressure sensitivity can be written as in Eq. (15) (Ref. 23) where p_{ij} are the strain-optic coefficients and n_e is the effective refractive index of the fiber laser.

$$\begin{aligned} \begin{bmatrix} P_4 \\ Q_4 \end{bmatrix} &= [T_s][T_1][T_2][T_3][T_4][T_5][T_d] \begin{bmatrix} P_3 \\ Q_3 \end{bmatrix} \\ &= \begin{bmatrix} T_{11} & T_{12} \\ T_{21} & T_{22} \end{bmatrix} \begin{bmatrix} P_3 \\ Q_3 \end{bmatrix}, \end{aligned} \quad (13)$$

$$\varepsilon = \frac{j3.24(T_{11} - e^{j\theta})}{\omega L_f S_d T_{12}} P_3, \quad (14)$$

$$\eta = \left\{ 1 - \frac{n_e^2}{2} [p_{12} - \nu(p_{11} + p_{12})] \right\} \varepsilon. \quad (15)$$

The frequency response of the pressure compensation scheme can be derived using Eqs. (12) and (13) as a ratio of the diaphragm chamber pressure to the external pressure as expressed in Eq. (16).

$$H(\omega) = 1 - \left(\frac{e^{j\theta} - T_{11}}{T_{12}}\right) \left(\frac{j\omega M_d + R_d - K_{eff}}{S_d^2}\right). \quad (16)$$

The sensor model expressed in Eqs. (15) and (16) can be used for the optimization of the design parameters. To achieve the design objectives, the fundamental natural frequency and pressure sensitivity values of the systems were chosen to be more than 7.5 kHz and $2 \times 10^{-9} \text{ Pa}^{-1}$, respectively. A parametric study was performed by varying the

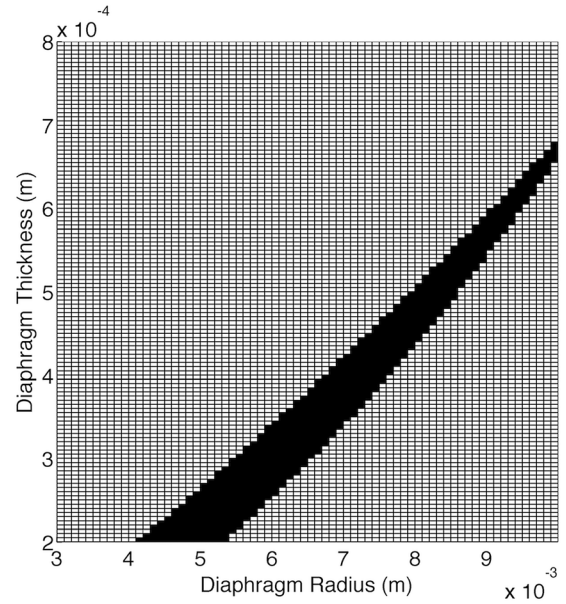


FIG. 4. Effect of diaphragm dimensions on the sensor performance. The black colored region of the graph satisfies the requirements on sensitivity and fundamental natural frequency.

thickness and the radius of the diaphragm. Figure 4 shows the results from the parametric study and the region marked black represents the acceptable operating points for which the natural frequency and sensitivity values met the design requirements. The dimensions of the prototype were then selected based on engineering requirements of pre-tension arrangement, slider sealing, ease of assembly and ease of fabrication. The prototype sensor employs a metal diaphragm of 0.35 mm thickness and 7 mm radius and has an overall diameter of 20 mm and length of 55 mm. Theoretical model was also used to fine tune the dimension of the acoustic filter used in the pressure compensation arrangement. Figure 5 shows the transmission characteristics of the pressure compensation scheme obtained using Eq. (16). As can be seen from the plot, pressure compensation scheme allows the equalization and diaphragm chamber pressure at

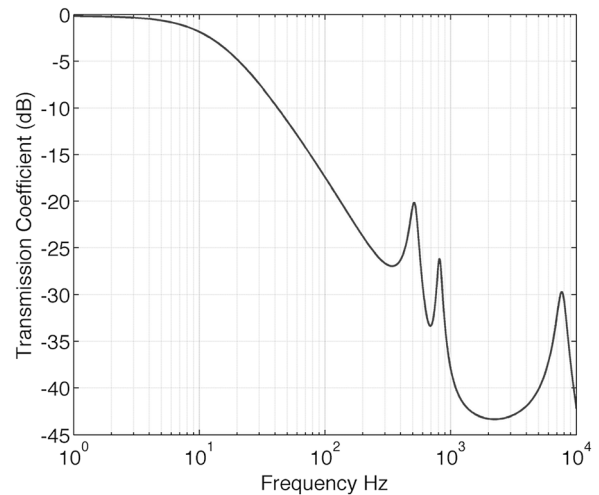


FIG. 5. Frequency response characteristics of the pressure compensation scheme.

frequencies below 5 Hz and the attenuates pressure variations happening at higher frequencies. The peak observed around 7500 Hz corresponding to the diaphragm resonance and the peaks around 500 Hz and 800 Hz corresponding to cavity resonances of the acoustic filter get attenuated by more than 20 dB due to the effect of radiation resistance at the slider and viscous losses in the acoustic filter. Figure 6 shows the simulated frequency response characteristics of the prototype. A flat frequency response within ± 1 dB with linear phase response characteristics is predicted in frequency range 10 Hz to 5 kHz.

E. Performance prediction: FEA

Finite element analysis (FEA) of the proposed design configuration was carried out using ABAQUS software to validate the results obtained from simplified theoretical model and to further optimize the design parameters. Figure 7 shows the axi-symmetric finite element model of the DFB FL based hydrophone. Analysis was performed in two stages. In the first stage a static analysis was performed to incorporate the effect of pretension in to the analysis, which was then followed by a steady state dynamic analysis. Fluid structure interaction effects between sensor shell and fluids (air in side the cavity and surrounding water) were taken into account in the model to include the effects of fluid loading on the sensor and radiation losses. The viscous losses in the acoustic filter were modeled using volumetric drag property of acoustic medium available in ABAQUS software. Volumetric drag is defined as the force experienced by acoustic medium per unit volume per unit velocity. The theoretical values of flow resistance obtained for each element of the acoustic filter using Eq. (4) were applied to corresponding domain in the finite element model. Plane wave excitations were applied on the sensor using acoustic

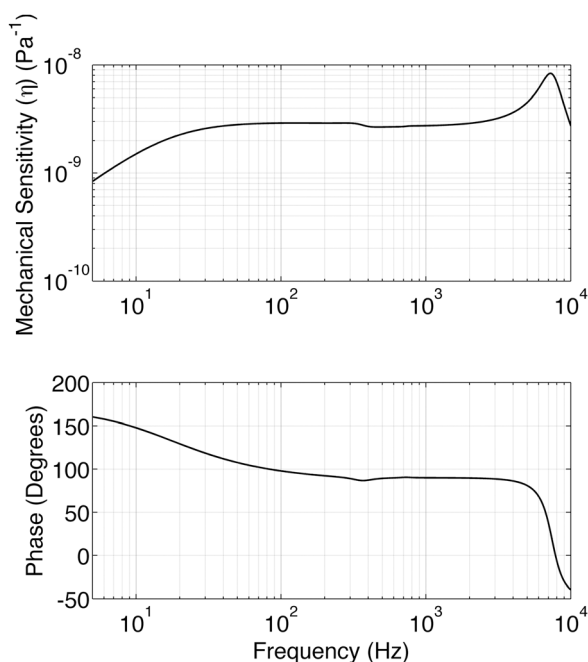


FIG. 6. Frequency response characteristics prediction from theoretical model.

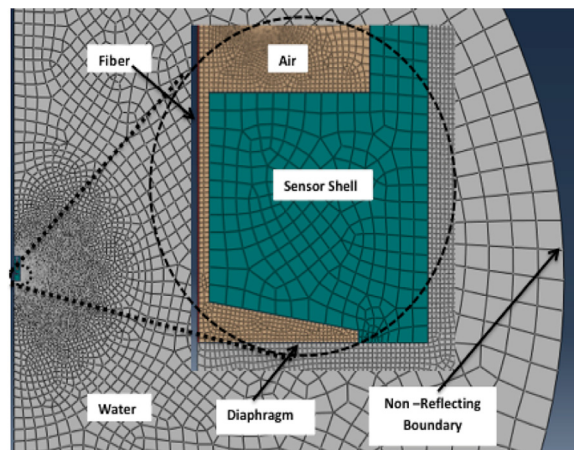


FIG. 7. (Color online) FEA model.

propagation models available in ABAQUS. Non-reflecting impedance boundary condition was applied on the outer boundary of external fluid domain and a scattered wave formulation was used in the analysis. Steady state dynamic analysis was carried out over the frequency range of interest to predict the sensitivity and frequency response characteristics of the sensor. Figure 8 shows the scattered pressure distribution around the sensor for a plane wave excitation at 4100 Hz and amplitude of 1 Pa.

Figure 9 shows the comparison between the FEA results and the frequency response predicted by simplified theoretical model. It can be observed that the simplified theoretical model accurately predicts the response of the sensor system. The resonance frequency and peak amplitude predicted by the simplified analytical model deviates marginally from the results obtained from the FEA. The natural frequency predicted by the analytical model is higher as the simplified theoretical model of the diaphragm neglects actual geometry and the effects of epoxy molding at the center of the diaphragm, which introduces additional mass and reduction in stiffness of the diaphragm. It was also observed that the changes in diaphragm resonance with pretension in the fiber was negligible and the bending stiffness of the diaphragm is

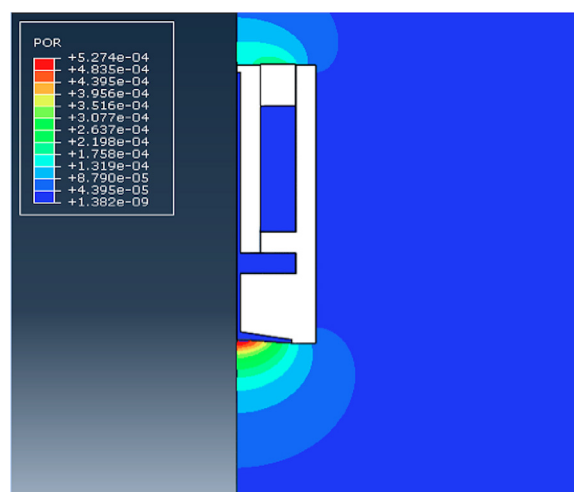


FIG. 8. (Color online) Scattered pressure amplitude (in KPa) distribution from axisymmetric finite element analysis.

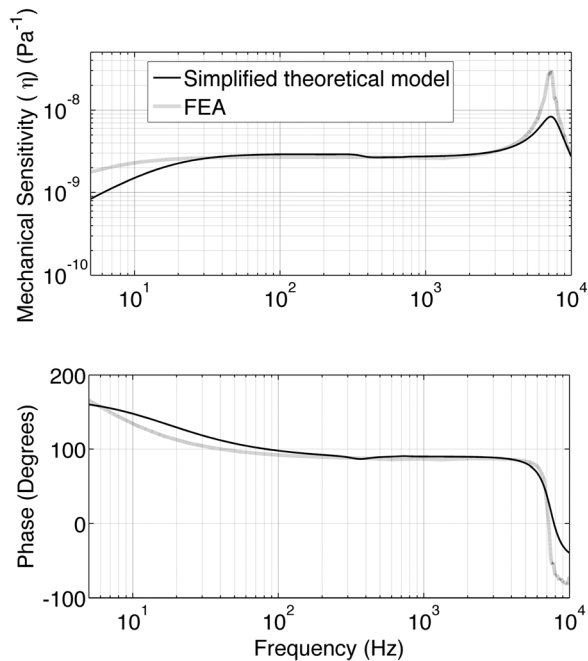


FIG. 9. Comparison between theoretical and FEA results.

the major parameter that controls the strain sensitivity as well as the natural frequency for the proposed configuration. Acoustic radiation by a diaphragm mounted on an infinite baffle is used for the estimation of the radiation loss in the simplified model. This differs from the actual scenario and over predicts the losses at the diaphragm and results in a flatter response at the fundamental resonance.

V. EXPERIMENTAL RESULTS

A. Pressure compensation scheme

The effectiveness of the pressure compensation arrangement was tested through hydrostatic pressure tests. Two different sensor configurations, one with pressure compensation scheme and the other without pressure compensation scheme, were subjected to hydrostatic pressures and corresponding changes in the wavelengths of the fiber laser were measured using an optical spectrum analyzer with a wavelength resolution of 0.001 nm.

The results from the experiments are plotted in Fig. 10. The measurements for the sensor without pressure compensation were limited to a depth of 11 m as at higher pressures the sensor showed a non-linear response. Experimental results showed that the shift in the wavelength of the fiber laser corresponding to the static pressure is negligible for operational depths of up to about 43 m, which is approximately 6 m lower than the theoretically value. This difference is possibly due to a mismatch in the slider chamber volume accounted for in the computation and the actual volume. The operational depth range of the pressure compensation scheme can be further increased depending on the operational requirement by providing additional volume in the slider chamber and by further optimization of diaphragm chamber volume.

The effects of friction at the O-ring sealing between the slider and the slider chamber walls could also be observed in

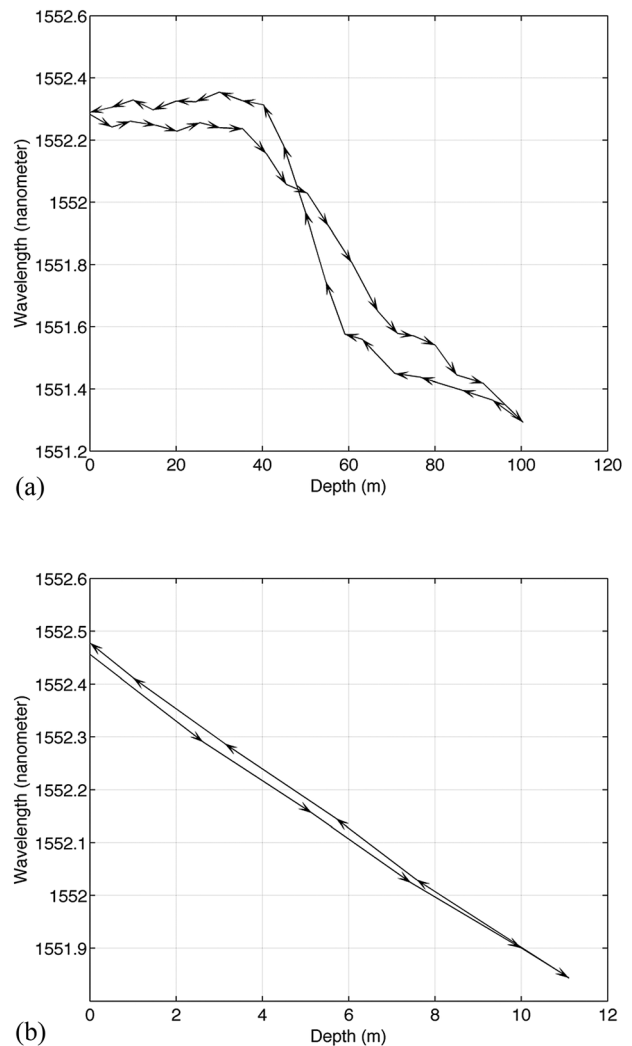


FIG. 10. Experimental results from hydrostatic testing. (a) The variation of fiber laser wavelength with hydrostatic pressure for a pressure compensated sensor prototype and (b) the similar results for a prototype sensor without pressure compensation.

the test results. The stick-slip friction at the O-ring sealing in the chamber is possibly the main contributor to the wavy nature of the wavelength variations with external hydrostatic pressure. The difference in the wavelengths for the depth range 0–40 m during pressure increase and decrease is also partially linked to the friction effects.

B. Acoustic test

The experimental set up used to evaluate the acoustic characteristic of the DFB-FL hydrophone is shown in Fig. 11. A Mach Zehnder interferometer configured with 1 m path imbalance and a piezo-ceramic fiber stretcher was used in the measurement. The phase demodulator, OPD4000 from Optiphase, employed a phase generated carrier (PGC) demodulation technique as detailed in Ref. 24. Frequency dependent sensitivity of the pressure compensated fiber laser hydrophone in the frequency range 0.8–10 kHz were evaluated in a 2 m × 2 m × 2 m acoustic tank using pulse excitations to eliminate the effect of acoustic modes of the tank on the measurement results. The low frequency measurement

fiber laser hydrophone showed negligible variation in the wavelength with static pressure for operational depths up to 40 m, which could be further improved by increasing the slider chamber volume of the proposed fiber laser hydrophone encapsulation. The acceleration sensitivity measurements in air showed that the sensor has an acceleration rejection figure of 0 dB ref m/s²/Pa. The prototype sensor has also been characterized for its frequency dependent sensitivity in a small acoustic tank. The experimental results appear to be in good agreement with the theoretical predictions.

ACKNOWLEDGMENTS

We thank I²R, A-STAR Singapore for fabricating the DFB-FL sensor toward experimentation and validation under a research collaboration.

- ¹C. R. Batchellor and C. Edge, "Some recent advances in fiber-optic sensors," *IEEE J. Electron. Commun. Eng.* **2**, 175–184 (1990).
- ²A. D. Kersey, *Distributed and Multiplexed Fiber Optic Sensors* (John Wiley and Sons, Hoboken, NJ, 2011), Chap. 9, pp. 277–314.
- ³M. Dignonnet, B. Vakoc, C. Hodgson, and G. Kino, "Acoustic fiber sensor arrays," *Proc. SPIE* **5502**, 39–50 (2004).
- ⁴D. Hill, P. Nash, D. Jackson, D. Webb, S. O'Neill, I. Bennion, and L. Zhang, "Fiber laser hydrophone array," *Proc. SPIE* **3860**, 55–66 (1999).
- ⁵A. Cusano, S. d'Addio, A. Cutolo, M. Giordano, S. Campopiano, M. Balbi, and S. Balzarini, "Plastic coated fiber bragg gratings as high sensitivity hydrophones," in *5th IEEE Conference on Sensors* (IEEE, Daegu, Korea, 2006), pp. 166–169.
- ⁶L. Hansen and F. Kullander, "Modelling of hydrophone based on a dfb fiber laser," in *Proc. of 21st ICTAM* (Springer Verlag, New York, 2005), pp. 15–21.
- ⁷W. Zhang, Y. Liu, F. Li, and H. Xiao, "Fiber laser hydrophone based on double diaphragms: Theory and experiment," *J. Lightwave Technol.* **26**, 1349–1352 (2008).
- ⁸I. Bedwell and D. Jones, "Fiber laser sensor hydrophone performance," in *OCEANS 2010 IEEE Sydney* (Sydney, Australia, 2010), pp. 1–5.
- ⁹S. Foster, A. Tikhomirova, M. Milnes, J. van Velzena, and G. Hardy, "A fiber laser hydrophone," *Proc. SPIE* **5805**, 627–630 (2005).
- ¹⁰S. Goodman, A. Tikhomirov, and S. Foster, "Pressure compensated distributed feedback fiber laser hydrophone," *Proc. SPIE* **7004**, 700426 (2008).
- ¹¹S. Foster, A. Tikhomirova, and J. van Velzena, "Towards a high performance fiber laser hydrophone," *J. Lightwave Technol.* **29**, 1335–1342 (2011).
- ¹²C. K. Kirkendall and A. Dandridge, "Overview of high performance fiber-optic sensing," *J. Phys. D* **37**, R197–R216 (2004).
- ¹³P. H. Dahl, J. H. Miller, D. H. Cato, and R. K. Andrew, "Underwater ambient noise," *Acoust. Today* **3**, 23–33 (2007).
- ¹⁴A. Dandridge, A. Tveten, and T. Giallorenzi, "Homodyne demodulation scheme for fiber optic sensors using phase generated carrier," *IEEE J. Quantum Electron.* **18**, 1647–1653 (1982).
- ¹⁵H. Jun, W. Lin, L. Fang, and L. Yuliang, "An ameliorated phase generated carrier demodulation algorithm with low harmonic distortion and high stability," *J. Lightwave Technol.* **28**, 3258–3265 (2010).
- ¹⁶Y. Liu, L. Wang, C. Tian, M. Zhang, and Y. Liao, "Analysis and optimization of the pgc method in all digital demodulation systems," *J. Lightwave Technol.* **26**, 3225–3233 (2008).
- ¹⁷J. Snowdon, "Mechanical four-pole parameters and their application," *J. Sound Vib.* **15**, 307–323 (1971).
- ¹⁸F. Fahy, *Foundations of Engineering Acoustics* (Academic Press, London, 2013), Chap. 7, pp. 149–155.
- ¹⁹F. Tarawneh and S. Muafag, "Friction forces in o-ring sealing," *Am. J. Appl. Sci.* **2**, 626–632 (2005).
- ²⁰L. Kinsler, A. Frey, A. Coppens, and J. Sanders, *Fundamentals of Acoustics* (John Wiley and Sons, New York, 2000), Chap. 7, pp. 184–187.
- ²¹W. Young and R. Budynas, *Roark's Formulas for Stress and Strain* (McGraw-Hill, New York, 2002), Vol. 6, Chap. 11, pp. 455–493.
- ²²L. Kinsler, A. Frey, A. Coppens, and J. Sanders, *Fundamentals of Acoustics* (John Wiley and Sons, New York, 2000), Chap. 4, pp. 107–109.
- ²³R. Kashyap, *Fiber Bragg Gratings* (Academic Press, Boston, MA, 2010), Chap. 10, pp. 443–444.
- ²⁴I. Bush and A. Cekorich, "Demodulator and method useful for multiplexed optical sensors," U.S. Patent 5,903,350 (May 11, 1999).